The Mistral base case to validate kinetic and fluid turbulence transport codes of the edge and SOL plasmas

Guilhem Dif-Pradalier, J Gunn, Guido Ciraolo, C Chang, Guillaume Chiavassa, P Diamond, Nicolas Fedorczak, Philippe Ghendrih, L Isoardi, M Kocan, et al.

Journal of Nuclear Materials xxx (2011) xxx–xxx

Contents lists available at ScienceDirect

Journal of Nuclear Materials

journal homepage: www.elsevier.com/locate/jnucmat

The Mistral base case to validate kinetic and fluid turbulence transport codes of the edge and SOL plasmas

G. Dif-Pradalier [a,**], J. Gunn [b], G. Ciraolo [c], C.S. Chang [d], G. Chiavassa [c], P. Diamond [a], N. Fedorczak [b], Ph. Ghendrih [b,*], L. Isoardi [c], M. Kocan [b], S. Ku [d], E. Serre [c], P. Tamain [b], Tore Supra Team [b]

[a] Center for Astrophysics and Space Sciences, UCSD, La Jolla, CA 92093, USA
[b] CEA, IRFM, F-13108 Saint Paul lez Durance, France
[c] M2P2, UMR 6181-CNRS, 38 Rue F. Joliot-Curie, 13451 Marseille, France
[d] Courant Institute of Mathematical Sciences, N.Y. University, New York, NY 10012, USA

ARTICLE INFO

Article history:
Available online xxxx

ABSTRACT

Experimental data from the Tore Supra experiments are extrapolated in the SOL and edge to investigate the Kelvin–Helmholtz instability. The linear analysis indicates that a large part of the SOL is rather unstable. The effort is part of the set-up of the Mistral base case that is organised to validate the codes and address new issues on turbulent edges, including the comparison of kinetic and fluid modelling in the edge plasma.

1. Introduction

The issue of transport in the edge region of fusion plasmas is among the most difficult and most crucial issue in understanding the operation of present devices and hence to predict that of ITER. Recent simulations with the code TOKAM-3D [1] have shown that when self-consistent turbulent transport was simulated one could recover the large-scale parallel flows that are observed in the experiments. Various global 3D simulation codes are presently in operation including fluid representations and gyrokinetic representations. As has been achieved for core turbulence [2], there is now a growing need to determine a reference base case in order to provide a means to both compare the codes (benchmarking) but also validate them. In particular, it is important to assess the role of the kinetic effects in the physics of the edge, SOL and divertor. It is clear that a divertor configuration will have to be considered for such a purpose. However, such simulations are demanding for the present state of the art modelling effort since the cold plasma that builds-up in the divertor leads to very small Larmor radii. Because the characteristic scales of turbulent eddies are governed by the Larmor radius, $k_\perp \rho_l \sim 0.3$, very large meshes are required, following typically a ρ^{*-3} scaling. The Tore Supra experiments provide an interesting alternative. First the circular geometry allows one to simplify the magnetic geometry, second the relatively hot plasmas are less demanding regarding the ρ^* values and therefore the mesh size, third, there is a wealth of very interesting observations that relate turbulence, transport and the choice of the limiter configuration with very small changes of the magnetic equilibrium. Last and not least, Tore Supra is characterised by significant ripple that can be varied with a proper positioning of the plasma within the chamber. This provides a means to modify the plasma toroidal rotation while maintaining most other parameters constant [3,4]. Together with appropriate diagnostics, this offers a unique opportunity to investigate plasma rotation and validate the modelling effort. The latter point is all the more important that rotation shear of the plasma is understood to be a key player of the barrier formation [5], the H-mode remaining to be consistently modelled.

2. The physics of the Mistral base case

The Tore Supra experiments that we consider in the Mistral base case have the following common characteristics. Magnetic surfaces are circular with typical major radius $R \sim 2.4$ m, minor radius $a \sim 0.7$ m, elevation with respect to the midplane $z \sim 0$ m, toroidal magnetic field $B_\varphi = 2$–4 T and plasma current $I_p = 0.6$–1 MA.

2.1. Magnetic equilibrium

The toroidal field is generated by $N_{\rm coil} = 18$ identical circular coils $R_{\rm coil} = 2.2$ m, inner minor radius $a_{\rm coil} = 1.154$ m (radial thickness $\Delta a_{\rm coil} = 0.226$ m, each coil has $N_t = 2028$ turns, The ripple can be approximated by $\delta B_{r,\rm ripple} = \langle B_\varphi \rangle \sin(N_{\rm coil}\varphi_r)\ (-0.5\Delta_0) \exp[-(a_{\rm coil} - r_r)/\lambda_{\rm ripple} - (\theta_r/\theta_{\rm ripple})^2]$. Where $\delta B_{r,\rm ripple}$ is aligned along

* Corresponding author. Address: Bât 513/151, IRFM, CEA Cadarache, 13108 Saint Paul lez Durance, France.
** Presenting author. Address: Center for Astrophysics and Space Sciences, UCSD, La Jolla, CA 92093, USA.
E-mail addresses: gdifpradalier@ucsd.edu (G. Dif-Pradalier), philippe.ghendrih@cea.fr (Ph. Ghendrih).

0022-3115/$ - see front matter © 2011 Elsevier B.V. All rights reserved.
doi:10.1016/j.jnucmat.2010.12.035

the radial coordinate in the toroidal frame with major radius R_{coil} at the position $(r_r, \theta_r, \varphi_r)$ with $\theta_r = 0$ at the midplane low field, $\varphi_r = 0$ between two coils and $\lambda_{ripple} = 0.182$ m, $\theta_{ripple} = 5\pi/6$, and the maximum radial displacement governed by the ripple at the coil location is $\Delta_0 = 0.066$ m. The averaged toroidal field is $2\pi R\langle B_\varphi\rangle = \mu_0 N_{coil} N_t I_{coil}$, where I_{coil} is the coil current (ranging from 500 A to 1000 A). Within the precision of the measurements, the magnetic surfaces are circular with shifted magnetic surfaces depending on the Shafranov shift parameter $\Lambda = \beta_p + l_i/2$, with major radius $R_r = (R_a^2 + (a^2 - r^2)(1 + \Lambda))^{1/2}$, R_a being the major radius of the last closed magnetic surface with radius a. In this framework, the poloidal magnetic field can conveniently be approximated by $B_\theta = \langle B_\theta\rangle(1 + \Lambda\, r\cos(\theta)/R_r)$ where $2\pi r\langle B_\theta\rangle = \mu_0 I_p$. Analytical expression for the safety factor, holding for the outer plasma with vanishing plasma current, and intrinsic magnetic coordinates can then be calculated [6].

2.2. Reference cases

The four reference cases of the Mistral base case have been investigated in [4]. These limiter plasmas differ by the location of the main limiter. The limiters that have been used in these experiments are such that the limiter structure is quasi-axisymmetric so that in the modelling effort, axisymmetric limiters can be considered. The first case, labelled HFS for High Field Side, appears as a standard inner bumper configuration. The second case is a standard Tore Supra limiter configuration using the lower limiter (ion grad B drift being oriented downwards), it is labelled BOT. The third case, labelled LFS for Low Field Side, is limited by outer limiters, the plasma centre being at $z = 0$ to preserve up–down symmetry. Finally, the configuration labelled as TOP, in quasi-identical to the previous case, the contact point being shifted upwards on the outboard limiters so that the up–down symmetry is broken. These four configurations are analysed with a reciprocating probe with vertical displacement from a top port at major radius $R_{probe} \sim 2.55$ m. Very strong differences are reported for these experiments. First the e-folding length of density is typically 120 mm for the HFS configuration and 30 mm for the LFS configuration. Also, the parallel Mach number is oriented clockwise in the poloidal plane (positive) in the TOP configuration, but counter clockwise (negative) in both the HFS and BOT configurations. In the LFS configuration, the Mach number is small and clockwise. Last and not least, the magnitude of this flow is large, typically $M_{//} \sim 0.5$. First 3D turbulence simulations have allowed us to recover the sign and magnitude of the parallel flow in the standard BOT configuration [1]. Fluctuations measurements have been performed for these configurations [7,8]. These measurements indicate that the particle transport is ballooned on the outer midplane extending typically from $-50°$ to $50°$. Finally, ion temperature measurements have also been performed in [9]. In the latter paper in the BOT configuration, the ion temperature is of the order of 80 eV at the last closed flux surface, a factor 3 larger than the electron temperature, with e-folding lengths of order 41 mm for T_i and 32 mm for T_e. It is important to underline that these temperature measurements are defined as that of the background plasma between the bursts that govern transient increases of the temperature. The data analysed in the present paper has been obtained in a 3.8 T shot. At the probe location the hybrid Larmor radius $\rho_s = [(T_e + T_i)/m_i]^{1/2}/(eB/m_i)$, then ranges from $\sim$0.38 mm, $\rho^* = 5.3 \times 10^{-4}$, at the last closed magnetic surface to 0.12 mm, $\rho^* = 1.7 \times 10^{-4}$, at $r/a = 1.1$. The physics addressed in the present version of the Mistral base case have also been addressed in divertor configurations [10]. However, modelling the latter configuration adds all the complexity of divertor physics. The limiter experiments thus appear to be an appropriate reduced case to investigate the physics of edge flows.

3. Stepping from the local probe measurements to 2D background plasma

An important issue in the validation effort relies on using dimensionless parameters, such as ρ^*, as well as appropriate coordinates. Shaped plasmas have led to consider the poloidal magnetic flux as the appropriate radial coordinate. Regarding parallel transport, one finds that intrinsic magnetic coordinates, the angles θ^* and φ^*, are more appropriate since they are characterised by the following proportionality relations; $ds = q\, R_0\, d\theta^*$, and $ds = q\, R_0\, d\varphi^*$, where R_0 is a reference major radius constant on a magnetic surface and s the curvilinear abscissa. Proportionality between the connection length (along the s coordinate) and the angles is particularly powerful to address the effect of poloidally localised sources. Edge plasma physics are particularly difficult to diagnose in a comprehensive and coherent way. In the most optimistic case, one must consider a 2D description of the steady state plasma, steady state standing here for the time averaged plasma. Ripple and non-axisymmetric plasma facing components will govern 3D effects. However, measurements in the plasma boundary are localised poloidally and toroidally. Full torus, turbulence simulations of the edge and SOL plasma [1,11] will then have to match these local conditions. Similarly, transport simulations in the edge are being performed in the limiter configuration with the SOLEDGE-2D code [12,13] and aim at recovering these measurements by adjusting the transport coefficients for the transverse particle and momentum diffusion. It can be shown that for large enough temperatures, the plasma in limiter configurations tends to be isothermal in the parallel direction. However, ion and electron temperature physics are also presently included in this modelling effort [14]. We will consider here such background plasma together with an analytical description to analyse the Kelvin–Helmholtz stability of such plasmas. This specific interest is both governed by the need to gain insight in the physics of the edge flows and to investigate potential issues raised by instabilities generated in the vicinity of the limiters. The chosen approach adopted here is similar to the so-called onion skin modelling [15]. One assumes that the total plasma pressure $\Pi = n(T_e + T_i)(1 + M_{//}^2)$ is approximately constant along the field lines [12,13], so that the measurement of the saturation current $(e\, n\, c_s)$ and that of the parallel Mach number yield $\Pi/(m_i\, c_s)$ where c_s is the sound speed $(m_i c_s^2 = T_e + T_i)$. Reasonable assumptions on the source location and magnitude then allow one to extrapolate the local measurements to the whole SOL. For the sake of simplicity, we consider a piecewise transverse particle flux and assume that the variation of the Mach number is governed by this cross-field transport. This assumption is rather specific of limiter configurations where SOL recycling will tend to be small. Given the input from the experimental analysis, we assume that the ballooned transport extends from $-\theta^*_{bal}$ to θ^*_{bal} hence with up–down symmetry with respect to the outboard midplane [4,8], $\theta^{ast}_{bal} \sim 0.22\,\pi$ in intrinsic coordinate θ^*, see Fig. 1. The probe is located approximately at $\theta^*_{probe} \sim 0.45^*\pi$ while the bottom limiter is located at $\theta^*_{lim} \sim -0.45^*\pi$. Following the formalism presented in [16], one can relate the particle flux to the integral of the source term $\Gamma(\theta^*) = \int_0^{\theta^*} dsS$. Using the appropriate angle θ^* then allows one to determine the parallel particle flux at the limiter, in both the co and counter direction and at the probe location:

$$\Gamma^+_{\rm lim} = [S_{bal}(\theta^*_{bal} + \theta^*_{stag}) + S_{unif}(-\theta^*_{\rm lim} + \theta^*_{stag})]qR_0 \tag{1a}$$

$$\Gamma^-_{\rm lim} = -[S_{bal}(\theta^*_{bal} - \theta^*_{stag}) + S_{unif}(2\pi - \theta^*_{\rm lim} - \theta^*_{stag})]qR_0 \tag{1b}$$

$$\Gamma_{probe} = -[S_{bal}(\theta^*_{bal} - \theta^*_{stag}) + S_{unif}(\theta^*_{probe} - \theta^*_{stag})]qR_0 \tag{1c}$$

The choice of the signs of the fluxes is done in agreement with the experimental definition of the sign of the Mach number. In this

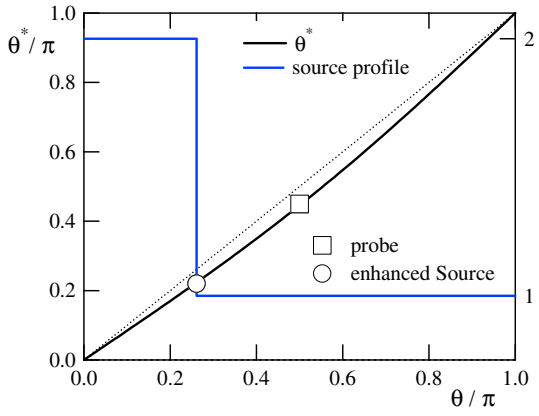

Fig. 1. Intrinsic angle θ^* versus the standard poloidal angle. The two crosses correspond to the extent of the enhanced ballooned transport region and to the location of the probe.

analysis θ^*_{stag} is the poloidal location of the stagnation point while S_{unif} is the uniform source and S_{bal} is the ballooned step increase of the source on the low field side. We assume here that the total plasma pressure is nearly constant along the field lines and introduce the control parameter $\mathcal{A}$ such that:

$$\mathcal{A} = \frac{2M}{1+M^2} = \frac{2\Gamma c_s}{\Pi/m_i} \tag{2}$$

where c_s is the sound velocity and Π the total plasma pressure. This parameter weighs the relative contribution of the parallel variation of the Mach number $\partial_s M$ and that of the density $\partial_s \mathrm{Log}(n)$ in the variation of the total plasma pressure Π. At the limiter, one readily finds $\mathcal{A} = \pm 1$ while at the probe one can compute $\mathcal{A}$ given the Mach number measurements. The constant Π and constant c_s approximation, supported in [13,14], then allows one to obtain two constraints and then determine the peaking factor of the ballooned transport S_{bal}/S_{unif} as well as the location of the stagnation point θ^*_{stag}, Fig. 2. Given the shape and location of the ballooned source term as well as its peaking factor, it is then possible to map the probe measurement on the total SOL. A 2D plot of parameter $\mathcal{A}$ together with profiles of $\mathcal{A}$ and of the density at the probe location are shown on Figs. 3a and b. Two parts in the extension of the data are shown, the parallel extension and a radial extension into the edge plasma. An exponential decay of $\mathcal{A}$ is chosen into the plasma edge that governs a rapid smoothing of the density in the poloidal direction as well as a decrease of the Mach number in the plasma edge. This

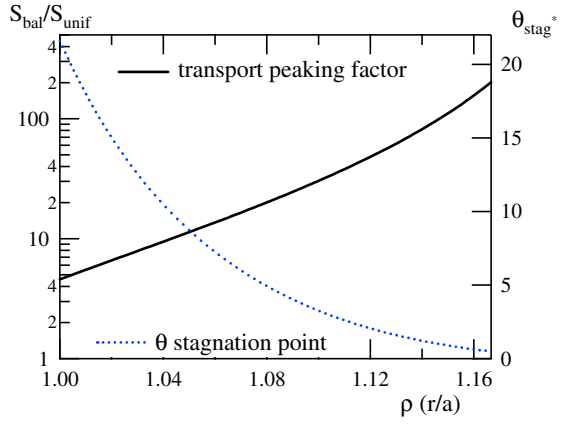

Fig. 2. Peaking of the ballooned transport with respect to the uniform background transport and location of the stagnation point.

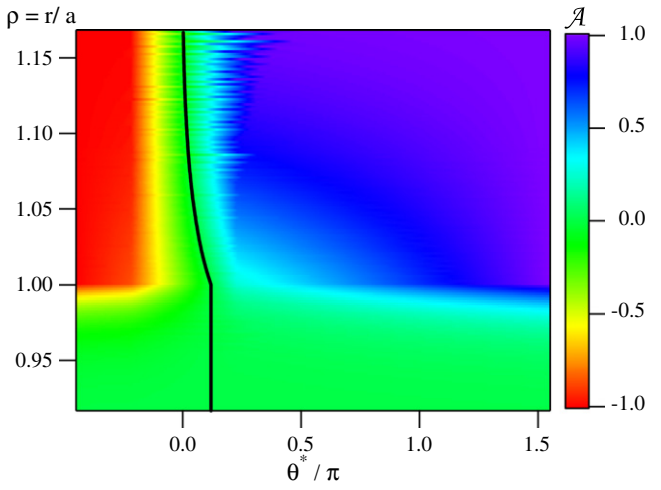

Fig. 3a. 2D plot of the parameter $\mathcal{A}$, The black curve corresponds to the $\mathcal{A} = 0$ line.

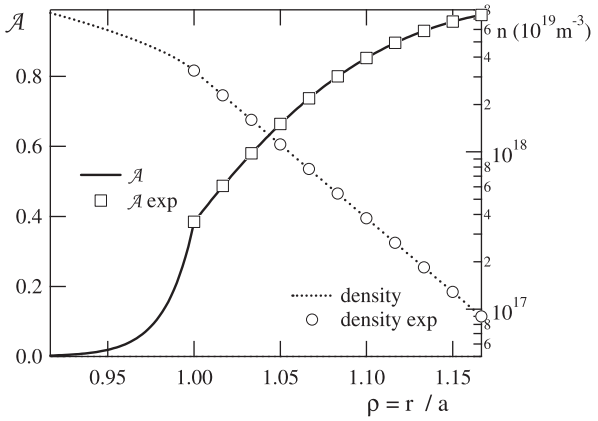

Fig. 3b. Profiles of the control parameter $\mathcal{A}$ at the probe location, experimental data and extrapolation into the plasma edge.

radial extrapolation is not backed by experimental data, at this stage it is only a reasonable assumption.

4. Local stability analysis of Kelvin–Helmholtz instability

Several instability mechanisms have been analysed in the edge and SOL plasmas [17,18]. Of particular interest is the Kelvin–Helmholtz instability driven by gradients of the parallel flow velocity [19] in both experiments and in the modelling effort [11]. The extrapolation of the experimental data obtained in Section 3 is used here to determine a value of one of the critical parameters that drive the onset of the Kelvin–Helmholtz instability. The Schmidt parameter is defined as the ratio of the momentum diffusion coefficient $\nu_\perp$ and of the particle diffusion coefficient $D_\perp$ in the transverse direction, $Sc = \nu_\perp/D_\perp$. These parameters are effective coefficients governed by turbulence (in particular $D_\perp$ is undefined for collisional transport). In practise, these coefficients thus depend on the turbulent transport that will include Kelvin–Helmholtz turbulence. In the spirit of the linear analysis, one should consider only the subgrid transport and turbulent transport not stemming from the Kelvin–Helmholtz instability. This cannot be achieved when considering experimental data. Rather than seeking to extrapolate these coefficients from the present data, we evaluate the required Schmidt parameter to trigger the instability. The linear analysis, assuming scale separation between the unstable

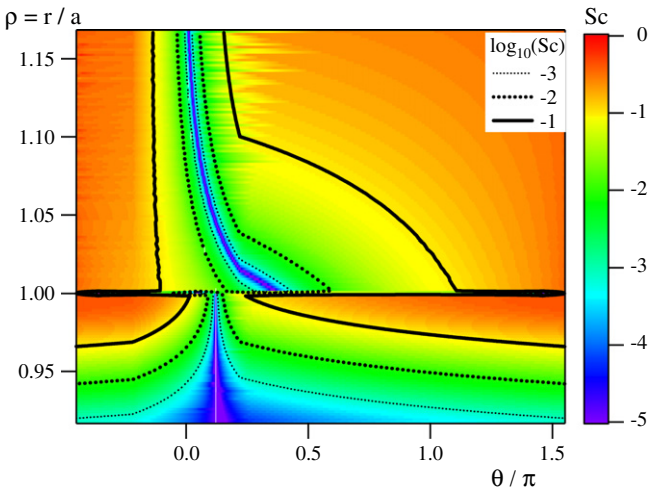

Fig. 4. 2D map in the ρ, θ^* plane of the Schmidt parameter required to destabilise Kelvin–Helmholtz modes. For $Sc \leqslant 0.1$ most of the SOL away from the stagnation point is unstable. The edge layer close to the SOL appears to be the most unstable.

modes and the gradients that drive the instability [11], then allows one to calculate the Schmidt parameter that will exhibit unstable Kelvin–Helmholtz turbulence. One then finds the following necessary condition:

$$Sc^2 - 2(1 + G/2)Sc + 1 > 0 \tag{3a}$$

$$G = \left[\left(\frac{dLog(n)}{dr}\right)^2 - \left(\frac{dM}{dr}\right)^2\right]\left(\frac{d\Gamma}{ndr}\right)^{-2} \tag{3b}$$

One readily finds that both $Sc << 1$ and $Sc >> 1$ branches are possible. We consider here the situation such that the Schmidt parameter tends to be small, weak viscosity compared to particle diffusion. One finds that for moderate values of the Schmidt parameter, typically $Sc < 0.1$, most of the SOL away from the stagnation point is unstable, Fig. 4. Furthermore, one finds that the edge region, in the vicinity of the separatrix appears to be the most unstable with respect to the Kelvin–Helmholtz instability. This is readily expected since this region exhibits the transition from the large parallel flows in the SOL to the small core and edge flows. However, since this transition in only estimated in this work, the present result is only qualitative.

5. Discussion and conclusion

In this paper, we have presented a first analysis of the Mistral base case. As such, the Mistral base case represents a challenge to both fluid and gyrokinetic codes. First, quantitative information will be required from the fluid codes although low collisionality regions are included in the simulation domain. Second, it is mandatory to take into account electron transport since adiabatic electrons do not drive any electrostatic cross-field transport of particles. Two global codes will be used to investigate these experiments. The code SOLEDGE-3D [11] has started running with this kind of background plasma. The goal is to investigate the Kelvin–Helmholtz instability in these limiter shots. The code XGCp [20], a gyrokinetic PIC code aiming at core, edge and SOL simulations is being modified to address the physics of the Tore Supra shots. The experimental analysis performed in this paper in order to generate a 2D axisymmetric plasma background provides a first analysis of the turbulent properties. Using a linear analysis, one can investigate the unstable regions in the edge and SOL plasma. The difficulty in estimating the Schmidt parameter using experimental evidence has led us to determine the required value to generate Kelvin–Helmholtz unstable modes. Schmidt values in the 0.1 range indicate that Kelvin–Helmholtz is likely to be unstable in such experimental setting. The MISTRAL base case together with the gyrokinetic code XGC and fluid code SOLEDGE-3D is a first step in the effort to develop a new generation of plasma-wall interaction simulation codes. It includes benchmarking and validation activity, open to all codes. The possibility to enrich the MISTRAL base case together with the code development and validation procedure is crucial as one step towards first principal simulations of edge plasma simulations of ITER.

Acknowledgements

This work is supported by the ANR Project ESPOIR and by the European Communities under the Contract of Association between EURATOM and CEA, was carried out within the framework of the European Fusion Development Agreement. The views and opinions expressed herein do not necessarily reflect those of the European Commission.

References

[1] P. Tamain et al., J. Nucl. Mater. 390–391 (2009) 347.
[2] G. Falchetto et al., Plasma Phys. Control. Fusion 50 (2008) 124015.
[3] X. Garbet et al., Phys. Plasmas 17 (2010) 072505.
[4] J.P. Gunn et al., J. Nucl. Mater. 363–365 (2007) 484.
[5] P.H. Diamond et al., Plasma Phys. Control. Fusion 47 (2005) R35.
[6] Ph. Ghendrih, Résonance du divertor ergodique, Report EUR-CEA-FC-1537, 1995.
[7] N. Fedorczak et al., J. Nucl. Mater. 390–391 (2009) 368.
[8] N. Fedorczak et al., this conference.
[9] M. Kocan et al., J. Nucl. Mater. 390–391 (2009) 1074.
[10] B. LaBombard et al., Phys. Plasmas 12 (2005) 056111.
[11] F. Schwander et al., this conference.
[12] L. Isoardi, J. Nucl. Mater. 390–391 (2009).
[13] H. Bufferand, this conference.
[14] L. Isoardi, this conference.
[15] P. Stangeby, in: The Plasma Boundary of Magnetic Fusion Devices, Institute of Physics publishing, Bristol and Philadelphia, 2000.
[16] E. Serre et al., this conference.
[17] N. Mattor et al., Plasma Phys. Control. Fusion 36 (1994) 1115.
[18] X. Garbet et al., Nucl. Fusion 31 (1991) 967.
[19] X. Garbet et al., Phys. Plasmas 6 (1999) 3955.
[20] C.S. Chang, S. Ku, Phys. Plasmas 15 (2008) 062510.